Energy and Power 2013, 3(5): 79-84
DOI: 10.5923/j.ep.20130305.01

Effect of H_2 Addition via Solar-Driven Electrolysis on the Performance and Emissions of a CI Engine

Garry I. Negroni[1], Ralph C. Aldredge[2,*]

[1]Institute for Transportation Studies, University of California, Davis, CA, 95616, USA
[2]Department of Mechanical and Aerospace Engineering, University of California, Davis, CA, 95616, USA

Abstract A vehicle-integrated photovoltaic system was used to produce a gaseous mixture of H_2, O_2 and steam, via alkaline electrolysis, for aspiration into an indirect-injection compression-ignition engine for the purpose of reducing soot opacity and hydrocarbon emissions. Aspiration of 0.516 ± 0.007 L/min of the H_2-O_2-steam mixture produced through electrolysis of aqueous potassium hydroxide was found to reduce soot opacity, hydrocarbon emissions and particulate matter during part-load dynamometer tests. Performance improvements under full-load conditions were observed. However, part-load performance at various engine speeds was found to decrease due to pre-mature auto-ignition of the aspirated gas.

Keywords Vehicle-integrated Photovoltaic, Alkaline Electrolysis, Indirect Injection, Compression Ignition, Particulate Matter, Hydrocarbons, Soot Opacity

1. Introduction

Solar energy is abundant, inexhaustible as long as the Earth exists, and in constant flux daily, while the sun is the fundamental energy source from which most other forms of energy are derived including biomass, wind, hydroelectric and fossil fuels[1-3]. Direct applications of renewable solar energy towards improving fossil-fuel combustion and reducing heat-engine emissions will become increasingly more important as we explore sustainable solutions to our transportation energy needs. Vehicle integrated photovoltaic (VIPV) electricity can be used to power loads directly or charge energy-storage devices for later consumption. Most applications of VIPV focus on enhanced propulsion, extended battery range for battery-electric vehicles[4], or reductions in auxiliary loads for hybrid-electric vehicles[5]. With space available on the rooftop of most every vehicle, VIPV arrays offer renewable electrical energy decoupled from the primary fuel conversion system.

The primary objective of the current work is the implementation and evaluation of solar-driven electrolysis as a means for improving the performance and emissions of a light-duty vehicle; specifically, an indirect-injection (IDI) compression-ignition (CI) engine. In comparison with the direct-injection (DI) engine, the indirect-injection (IDI) compression-ignition (CI) engine is often preferred for light-duty applications because of its lower nitrogen-oxide (NOx) emissions, wider speed range and quieter operation, with minimal pumping losses[6]. In addition, the IDI CI engine more readily accommodates the consumption of biofuels, such as biodiesel or straight vegetable oil (SVO). Notwithstanding these attributes, the use of this engine is also generally hindered by its high hydrocarbon (HC) and particulate-matter (PM) emissions, due to relatively slow combustion processes.

The implementation of solar electrolysis exemplifies the direct application of renewable-energy technology in transportation, using solar energy as the primary energy source for improving IDI CI combustion of No. 2 diesel fuel. Earlier investigations of solar-driven electrolysis have typically involved application of the technology to large-scale systems[2, 7-9], while investigations of electrolysers used to improve CI engine combustion have often employed grid power rather than solar power for electrolysis, due to high power-input requirements[10, 11]. The present study incorporates aspects of each of these two approaches. The direct application of solar-driven electrolysis to a small-scale CI engine demonstrates a new avenue through which renewable, solar energy can be used in heat-engine powered vehicles that are decoupled from the electric grid.

The idea is to introduce a mixture of hydrogen, oxygen and water vapor produced onboard by solar-driven electrolysis into the cylinders of the IDI CI engine prior to ignition of the diesel-fuel. The combustion of hydrogen during the compression stroke, at approximately 849K, results in the production of heat, radicals and turbulence that all enhance the combustion of the diesel fuel when it is ignited shortly afterwards (when the piston is near top dead

* Corresponding author:
rcaldredge@ucdavis.edu (Ralph C. Aldredge)
Published online at http://journal.sapub.org/ep

center). Furthermore, the water vapor introduced into the cylinder as part of the mixture from the electrolyser gas, and that produced from the combustion of hydrogen, absorbs combustion heat and reduces the temperature in the cylinder, potentially resulting in reduced NOx emissions[6, 10-13].

2. Materials and Methods

Our test vehicle is a 1981 VW Rabbit MK2 DL with a biofuel-capable 1.6L MFI IDI CI engine and a 5-speed manual gearbox. The PV charging system consists of a single 180W Sharp PV Panel, a Morningstar Prostar-30 PWM charge controller, and two second-use 12V Optima Red Top lead-acid energy storage devices connected in parallel. The charging system and the energy storage device are connected in series. Figure 1 shows the layout of the VIPV system. National Instruments LabVIEW 2009 was used to acquire voltage and current data. Emano shunts (100A/100mV) were placed between the PV panel, the charge controller, and the energy storage devices. Voltage drops were measured across the shunts and current was measured across positive and negative terminals of the recipient device.

Figure 2 shows the structure of the electrolyser. It consists of 16-gauge 316L stainless-steel plates, 0.75-inch CPVC/Acrylic endplates and 16-gauge CPVC/Acrylic gaskets. Upon activation, the alkaline solution flows through the electrolyser at standard temperature and pressure. Power is delivered to the electrolyser directly and through a 45A DC chopper (12V at max), through 10-AWG stranded copper THHN. The average duty cycle (percentage time in active status) of the chopper was determined as the average power per cycle divided by the maximum power per cycle. An Emano (100A/100mV) shunt was placed between the energy storage device and the electrolyser, as shown in Fig. 3. The electrolysis test was conducted using potassium hydroxide (KOH) at its upper limit for remaining non-corrosive (2% by weight). Maintaining the electrolytic solution below corrosive levels increases plate longevity and permits safer consumer application. Flow rates were measured using a Gilibrator-2 Primary Air Flow Calibrator. Mass flow was initiated when a current was induced across the anodes and cathodes.

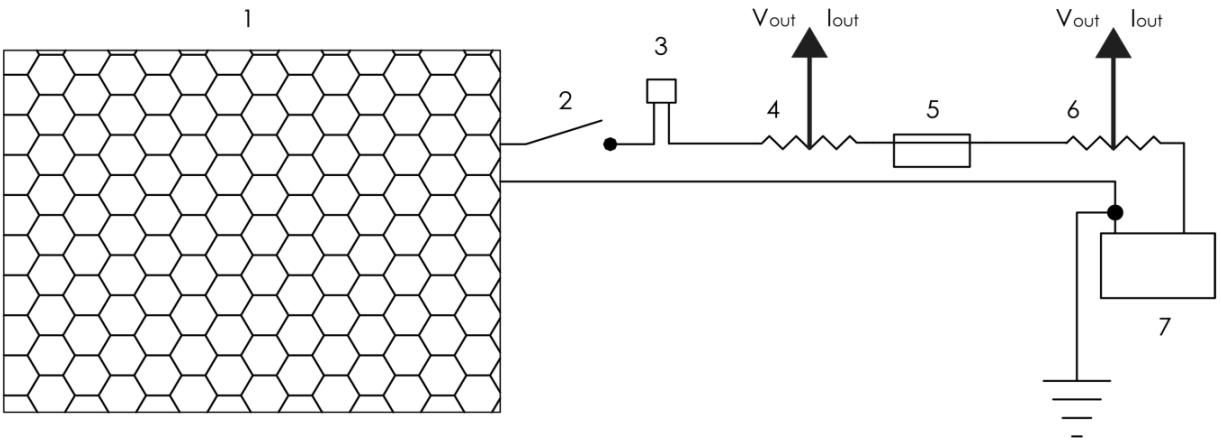

Figure 1. (Solar-PV charging system): (1) 180W Sharp PV Panel; (2) 600W Emergency Disconnect; (3) 30A Overcurrent Protection; (4,6) Emano 100A/100mV shunts; (5) Morningstar Prostar-30 PWM charge controller; (7) Second-use, 12V Optima Red Top sealed lead-acid batteries, connected in parallel

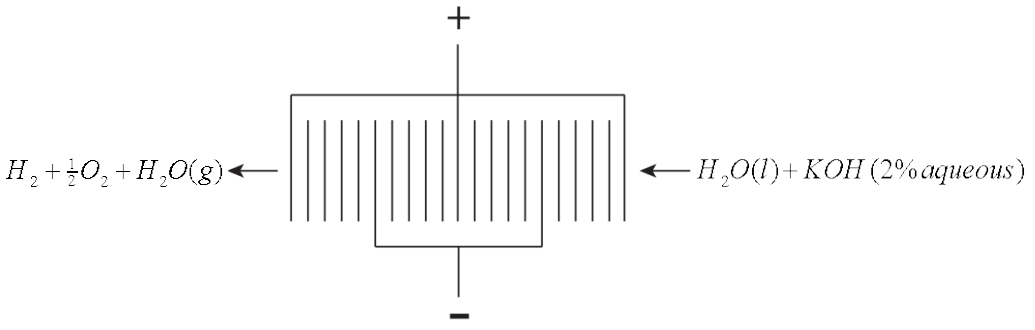

Figure 2. (Electrolyser): With three anodes and two cathodes connected in parallel, there are four bipolar plates in each stack, creating five cells per stack. The total active electrolyser surface area for 21 plates is 0.434 m^2

Average flow rates are correlated to average current inputs using a linear regression model obtained using the voltage efficiency, hydrogen energy density, and a stoichiometric hydrogen-oxygen ratio, in order to estimate the flow rate and energy content of hydrogen from the system for a given input current. This model was calibrated in accordance with energy conservation, given the power input to the system (i.e., the product of the thermo-neutral voltage per cell, the number of cells and the input current). Gas chromatograph measurements were taken from samples of the gas exiting the electrolyser[14] using a Varian 3800GC with thermal-conductivity and flame-ionization detection to determine the composition of the molecules exiting the electrolyser. Three 100μL samples were taken fifteen minutes apart after 5-8 minutes of operation prior to sample acquisition. The samples were acquired through the same sample vial in order to establish a mean while taking account for the saturation of the heavier oxygen molecules within the dry reservoir.

The Fuel mass per injection was determined by averaging the mass of single injections of diesel fuel from the MFI pump under full-throttle conditions. The average mass per injection was calculated and used to calculate the diesel energy input in the cylinder per injection. This value is then compared to the hydrogen energy input into the system per combustion event at various engine speeds based upon the mass air flow-rate per intake stroke.

Third-party opacity tests (also referred to as "free-acceleration tests") were conducted at California Diesel and Power, an emissions-testing facility in Martinez, CA approved by the California Air Resources Board (CARB). The Wager SAE J1667 Opacity Test used consists of three quick throttle flicks during which an infrared laser estimates the average opacity of tailpipe exhaust smoke. Tests were conducted for the baseline (with no vehicle modifications) and solar-electrolysis configurations, as shown in Fig. 4. In the solar-electrolysis configuration a solar photovoltaic array charges a separate energy storage device, independent of the vehicle's battery, which powers the electrolyser. The electrolyser produces a mixture of H_2, O_2 and steam, which is directed into the engine cylinders along with the diesel fuel.

Third-party dynamometer testing was conducted at the BRG Racing Dynamometer testing facility in Pacheco, CA. These tests were conducted with a Mustang MD-750 Eddy Current Dynamometer and included both part-load (step) testing and full-load (sweep) testing for the baseline and solar-electrolysis configurations. Power, torque and emissions were measured during part-load steady-state operation at several engine speeds with a wide-open throttle for the baseline and alternator-less cases. Emissions of carbon monoxide (CO), carbon dioxide (CO_2), oxygen (O_2) and hydrocarbons (HC) were measured, and voltages were recorded for all engine speeds tested. Hysteresis was observed in both tests with a significant delay observed in the flow rate response to power input, consistent with that reported in the literature[12]. Compensation for the delay was made using a delay factor derived from an energy balance. The duty cycle of the analog flasher characterizing the reduction of power from the energy storage device into the electrolyser during dynamometer and road tests (the ratio of average to peak power) was calculated to be 0.451.

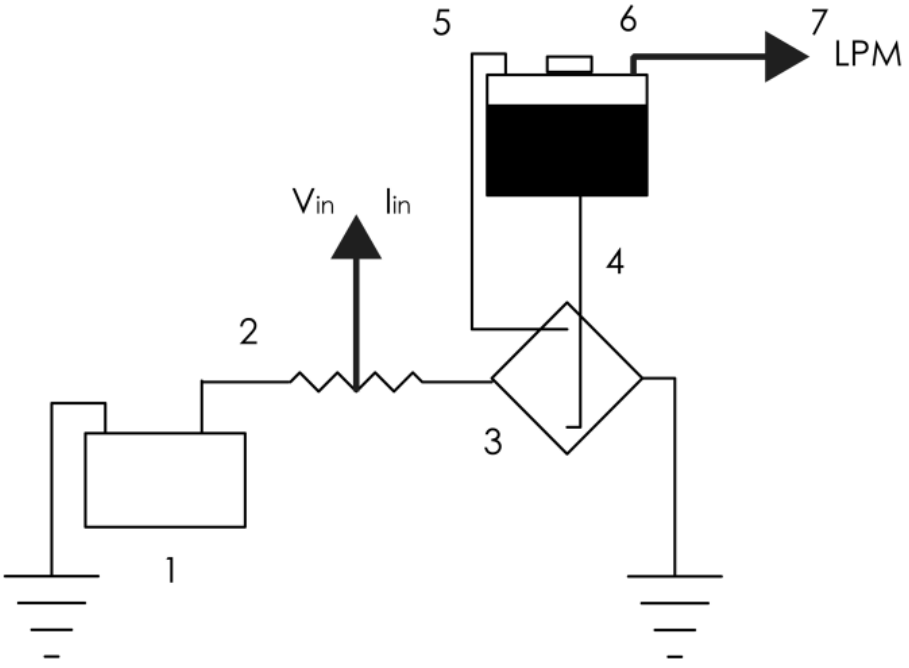

Figure 3. (Electrical component layout): (1) Energy storage; (2) Emano shunt; (3) Electrolyser; (4) Electrolyser inlet (liquid); (5) Electrolyser outlet (gas); (6) Reservoir outlet; (7) Flowmeter

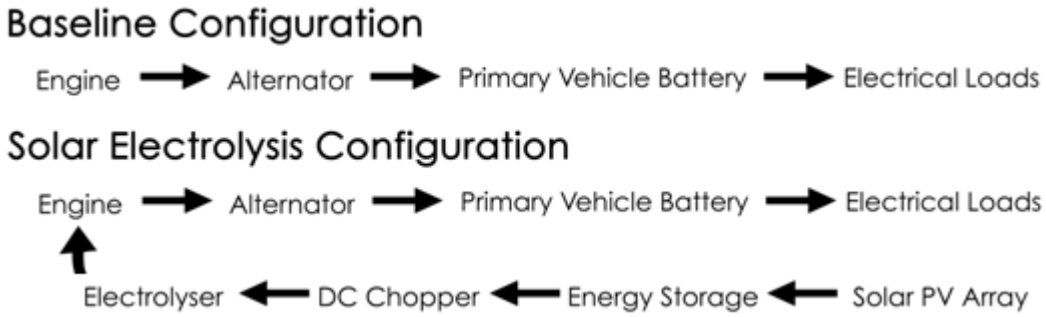

Figure 4. (Dynamometer test configurations): In the solar-electrolysis configuration a solar photovoltaic array charges a separate energy storage device, independent of the vehicle's battery, which powers the electrolyser

For the purpose of assessing the effectiveness of the VIPV system, we will assume an average daily solar insolation of 4 kWh/m^2. Considering the OEM-rated solar-panel efficiency of 13.6% then gives a possible solar-panel output of 544 Wh/m^2-day, on average. The total daily energy available from a vehicle-mounted PV system depends on the proportionally on the available area of the rooftop or appropriate PV panel. The PV panel used in our study has an area of 1.32 m^2 and can thus produce approximately 718 Wh/day (2.585 MJ/day). Therefore, with an average efficiency of 84.0% for the charge-controller used in our study (calculated from measured input and output voltage and current) the average solar-to-battery energy-conversion efficiency is then 11.7%, and the total energy available for delivery to the energy storage device is approximately 601.9 Wh.

3. Results & Discussion

With 2% (by weight) KOH, the electrolyser was able to produce 0.005 ± 0.0009 LPM/W at standard pressure and temperature. A linear regression model was used to correlate the input current I (in amperes) with the total flow rate in units of LPM (namely, $0.0523I - 0.0084$), accounting for 99.78% of the variation. The average flow rate of hydrogen based upon the thermoneutral voltage and the number of cells was found to be 0.0024 ± 0.0007 LPM, while the average current input was found to be 73 ± 1 mA/cm^2. The dependence of the electrolyser flow rate on the KOH concentration and the voltage and current input is used to determine the amount of hydrogen aspirated into the engine, based upon the voltage measurements and the operational electrolyser resistance. The average resistance, 0.698 ± 0.172 Ω, was used to calculate the power input to the electrolyser during road and dynamometer testing. Stoichiometric outputs for water electrolysis processes at the equilibrium voltage of 1.482V/cell are reported in the literature[2, 7-9, 15]. Voltage in excess of this value induces heat into the solution and the power at which this occurs is equivalent to system amperage times the difference between the actual cell voltage and the equilibrium voltage. Considering the average solar-to-battery energy-conversion efficiency of 11.7% and the average voltage efficiency of the electrolyser determined to be 69.2% during dynamometer testing, the solar-to-electrolysis efficiency is found to be 7.88%.

Table 1. GC Sampling From Electrolyser (%)

Test	H2	O2	ΔH2	ΔO2
1	99.06	0.93		
2	98.99	1.01	-0.07	0.07
3	98.31	1.69	-0.68	0.68
Stoic.	66.67	33.33		

Table 2. Chemical Power Input (%)

RPM	H2 (W)	Diesel (kW)	H2 / Diesel (%)
1500	13.3	542	2.5E-02
2000	9.62	723	1.3E-02
2500	7.56	904	8.0E-03
3000	6.30	1084	6.0E-03
3500	5.30	1265	4.0E-03
4000	4.64	1446	3.0E-03
4500	4.12	1626	3.0E-03
Average	7.26	1084	9.0E-03

Gas-chromatograph (GC) measurements taken at the exit of the electrolyser for each of three test runs are presented in Table 1, along with stoichiometric mole fractions for comparison. The mole fraction of H_2 (O_2) is defined as the ratio of the number of moles of H_2 (O_2) to the total number of moles of H_2 and O_2, excluding all other chemical species. The last two columns of Table 1 show mole-fraction variations found between consecutive test runs. Condensation was observed at the electrolyser reservoir outlet, indicating water vapor production, and there was observable bubble formation within the solution as well. However, testing limitations did not permit measurement of the amount of water vapor exiting the electrolyser. The disparity between the measured mole fractions and the stoichiometric values suggest the dissolution of oxygen into the electrolytic solution. This is supported by the greater solubility of oxygen in the electrolytic solution than that of hydrogen, the extent of which is exacerbated at lower temperatures but mitigated by the exothermicity of the

electrochemical reaction that can lead to higher temperatures. In fact, as the electrolyser cell warms with subsequent test runs, the mole fraction of oxygen in the electrolyser output is found to increase, as shown in Table 1. Appropriate temperatures must be achieved in order to approach stoichiometric output of H_2 and O_2 from the electrolyser. The assumption of stoichiometric electrolyser output is used to estimate the hydrogen content based on current input to the electrolyser during vehicle testing.

Table 2 shows a comparison of the power input to the engine independently attributable to the heating values of the H_2 and diesel fuel species. The power input associated with H_2 is calculated as the product of (a) the amount of H_2 introduced into the engine cylinder per cycle from the electrolyser (based on its current input), (b) the heat released from the combustion of H_2 with the aspirated air and (c) the engine speed. Since the amount of air aspirated into the engine per cycle increases with engine speed while the amount of H_2 introduced remains constant, the power input associated with H_2 is found to decrease monotonically with engine speed, as shown in Table 2. The power input associated with the diesel fuel, on the other hand, increases with engine speed, due to the increasing amounts of both airflow and injected diesel fuel with increasing speed. Consequently, the effectiveness of H_2 addition via solar-driven electrolysis decreases with increasing engine speed, as shown in Table 2.

Under full-load (sweep) dynamometer testing, H_2 addition resulted in an increase in peak engine power (torque) of 1.562% (2.608%) on average, over the range of engine speeds indicated in Table 2. Specifically, an additional 970W of engine power at full-load was gained from H_2 addition with an average of 7.26 ± 3.26 W, as a result of a solar-derived power input to the electrolyser of 107.4 ± 2.96 W. The significant gain in engine power beyond the solar-derived H_2 power input (a net of approximately 963W) can be attributed to improved diesel-fuel combustion as a result of H_2 addition. However, the effectiveness of H_2 addition diminishes with increasing engine speeds. This is because the flow rate of H_2 remains constant while the amount of diesel-fuel injected into the engine increases with increasing engine speed, resulting in a decrease in the amount of H_2 addition relative to the amount of diesel fuel burned (as shown in Table 2). Also, because hydrogen auto ignition and diesel injection occur closer in time with increasing engine speed, the increase in engine power resulting from H_2 addition is found to reach a maximum, found in our study at an engine speed of approximately 2900 RPM.

Table 3 summarizes the percentage changes in power, torque and emissions for each of the specified engine speeds selected for part-load (step) dynamometer testing with H_2 addition via solar-driven electrolysis. Under steady conditions at each of the selected engine speeds, H_2 addition resulted in a decrease in peak engine power and torque for all but the lowest engine speed tested (1500 RPM). On average (over the range of engine speeds indicated in Table 3), peak engine power (torque) was found to decrease by 3.67% (3.30%). This decrease is attributable to H_2 auto-ignition, which becomes prevalent under steady-state conditions at a fixed engine speed because cylinder temperatures are sustained closer to their peak, post-combustion levels in this case. On the other hand, the auto-ignition of even a small amount of hydrogen (0.009% of diesel fuel energy, on average) was found to result in reductions of HC and CO emissions during part-load (step) dynamometer testing, while CO_2 emissions were found to increase, potentially due to higher quantities of O_2 available during the combustion process. Reductions in HC emissions were greatest for engine speeds characteristic of typical daily driving (2000 - 3000 RPM). An SAE J1667 opacity test suggested an overall decrease in PM emissions, reflected in a decrease in opacity of 31.5% on average relative to baseline (without H_2 addition).

Table 3. Performance & Emissions with H_2 Addition Via Solar-Driven Electrolysis

RPM	ΔPower	ΔTorque	ΔCO	ΔCO2	ΔO2	ΔHC
1500	1.59%	2.29%	0.00%	4.95%	4.62%	200%
2000	-1.09%	-1.87%	0.00%	0.909%	0.769%	-34.8%
2500	-4.04%	-4.02%	0.00%	0.971%	-4.38%	-92.3%
3000	-7.30%	-4.15%	0.00%	1.87%	-4.38%	-95.2%
3500	-3.18%	-3.17%	0.00%	6.31%	-4.48%	33.3%
4000	-6.48%	-4.75%	-100%	-0.909%	-4.41%	75.0%
4500	-5.19%	-7.41%	-100%	3.77%	-5.80%	-70.8%
Ave.	-3.67%	-3.30%	-28.6%	2.55%	-2.58%	2.17%

4. Summary & Conclusions

Onboard solar-driven electrolysis for the production of an H_2-O_2-steam mixture to enhance diesel-fuel combustion was the focus of the current study. Under full-load (sweep) dynamometer testing, the addition of the H_2-O_2-steam mixture to the engine cylinder prior to diesel-fuel ignition was found to result in an increase in peak engine power (torque) of 1.562% (2.608%) on average, over a wide range of engine speeds (1500 - 4500 RPM). An additional 970W of engine power at full-load was gained from the addition of H_2 (at the level of 7.26 $\pm$ 3.26W), derived from solar-driven electrolysis. This net power increase of approximately 963W beyond the solar-derived H_2 power input can be attributed to improved diesel-fuel combustion as a result of H_2 addition. However, the effectiveness of H_2 addition was found to diminish with increasing engine speeds, reaching a maximum at an engine speed of approximately 2900 RPM.

Under part-load (step) dynamometer testing at steady state the addition of the H_2-O_2-steam mixture from the electrolyzer to the engine cylinder prior to diesel-fuel ignition was found to result in a decrease in peak engine power and torque for all but the lowest engine speed tested (1500 RPM). An average decrease in peak engine power (torque) by 3.67% (3.30%) is attributable to H_2 auto-ignition, which becomes prevalent under steady-state conditions at a constant engine speeds. Hydrogen addition was also found to result in reductions of HC and CO emissions and an increase in CO_2 emissions (likely due to a greater availability of O_2) under part-load (step) steady-state conditions. Reductions in HC emissions were greatest for engine speeds characteristic of typical daily driving (2000 - 3000 RPM). A decrease in opacity of 31.5% on average was found, suggesting an overall decrease in PM emissions as a result of H_2 addition via solar-driven electrolysis).

In conclusion, we have demonstrated the implementation of solar electrolysis as a direct application of renewable-energy technology in transportation, using solar energy as the primary energy source for improving IDI CI combustion of No. 2 diesel fuel. This implementation demonstrates a new avenue through which renewable, solar energy can be used in heat-engine powered vehicles that are decoupled from the electric grid.

ACKNOWLEDGEMENTS

We are grateful to Dr. Andrew Burke for assistance with testing during the study.

REFERENCES

[1] C. Flavin, and N. Lenssen, “Designing a sustainable energy system,” *Changing Environment Ideologies,* vol. 1, pp. 51, 1992.

[2] C. A. Grimes, O. K. Varghese, and S. Ranjan, *Light, water, hydrogen: the solar generation of hydrogen by water photoelectrolysis*: Springer, 2008.

[3] F. M. Vanek, and L. D. Albright, *Energy systems engineering*: McGraw-Hill, 2008.

[4] M. Fujinaka, “Solar cars free of environmental pollution—prototype of practically usable car completed,” *Renewable energy,* vol. 2, no. 1, pp. 57-64, 1992.

[5] D. Pile, “Photovoltaics: Solar-assisted cars,” *Nature Photonics,* vol. 3, no. 4, pp. 195-195, 2009.

[6] B. Challen, and R. Baranescu, "Diesel Engine Reference Book. 2nd," Butterworth-Heinemann Ltd. Pp, 1999.

[7] J. M. Bockris, B. Dandapani, D. Cocke, and J. Ghoroghchian, “On the splitting of water,” *International Journal of Hydrogen Energy,* vol. 10, no. 3, pp. 179-201, 1985.

[8] E. W. Justi, P. W. Brennecke, W. Schuh, and K. Claus, *A solar-hydrogen energy system*: Plenum Press, 1987.

[9] K. Rajeshwar, R. D. McConnell, and S. Licht, *Solar hydrogen generation: toward a renewable energy future*: Springer Science+ Business Media, 2008.

[10] S. Bari, and M. Mohammad Esmaeil, “Effect of H< sub> 2</sub>/O< sub> 2</sub> addition in increasing the thermal efficiency of a diesel engine,” *Fuel,* vol. 89, no. 2, pp. 378-383, 2010.

[11] A. C. Yilmaz, E. Uludamar, and K. Aydin, “Effect of hydroxy (HHO) gas addition on performance and exhaust emissions in compression ignition engines,” *international journal of hydrogen energy,* vol. 35, no. 20, pp. 11366-11372, 2010.

[12] K. Subramanian, “A comparison of water–diesel emulsion and timed injection of water into the intake manifold of a diesel engine for simultaneous control of NO and smoke emissions,” *Energy Conversion and Management,* vol. 52, no. 2, pp. 849-857, 2011.

[13] S. R. Turns, "An introduction to combustion. 2nd," Boston: McGraw Hill, 2000.

[14] L. Berben, and P. Serrano, Gas chromatograph testing conducted by P. Serrano of the UC Davis Berben research group., 2012.

[15] R. L. LeRoy, C. T. Bowen, and D. J. LeRoy, “The thermodynamics of aqueous water electrolysis,” *Journal of The Electrochemical Society,* vol. 127, no. 9, pp. 1954-1962, 1980.